Journal of Hazardous Materials 401 (2021) 123402

Contents lists available at ScienceDirect

Journal of Hazardous Materials

journal homepage: www.elsevier.com/locate/jhazmat

Carbon quantum dots-TiO_2 nanocomposite as an efficient photocatalyst for the photodegradation of aromatic ring-containing mixed VOCs: An experimental and DFT studies of adsorption and electronic structure of the interface

Asad Mahmood*, Gansheng Shi, Zhuang Wang, Zepeng Rao, Wang Xiao, Xiaofeng Xie, Jing Sun*

Shanghai Institute of Ceramics, Chinese Academy of Sciences, 1295 Dingxi Road, Shanghai 200050, China

GRAPHICAL ABSTRACT

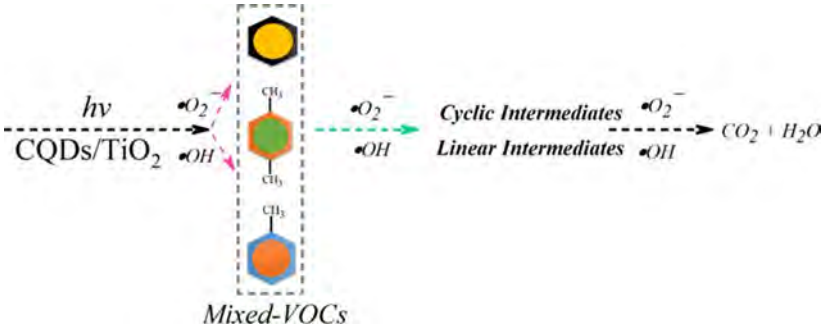

ARTICLE INFO

Editor: L. Eder

Keywords:
Oxide semiconductor materials
Photocatalytic oxidation
Carbon quantum dots
Volatile organic compounds

ABSTRACT

In this work, we have developed and optimized TiO_2 nanoparticles decorated with carbon quantum dots to examine its potential use in the photocatalytic oxidation of aromatic ring containing gas-phase mixed volatile organic compounds, e.g., benzene, toluene, and p-xylene. Carbon quantum dots decorated TiO_2 demonstrated good photodegradation efficiency in contrast to pure TiO_2 under UV–vis light illumination. For example, with 0.5 wt% carbon quantum dots decorated on TiO_2, 64 % of the mixed volatile organic compounds were photodegraded, while pure TiO_2 only exhibited 44 % of the photodegradation efficiency. Also, the carbon quantum dots (0.5 wt%)/TiO_2 nanocomposite demonstrated considerable photocatalytic activity within the visible region. On the other hand, pure TiO_2 remained inactive within the visible region. The density functional theory study of the carbon quantum dots/TiO_2 interface revealed that C 2p states of carbon quantum dots incorporated new energy states around the Fermi level near the lowest conduction band. This might be accountable for the improved charge separation process and better conductivity of the photogenerated electrons. The improved photocatalytic performance of the carbon quantum dots/TiO_2 nanocomposites can be attributed to good light harvesting within the UV–vis region, charge separation, and adsorption capability.

* Corresponding authors.
E-mail addresses: amkhan036@yahoo.com (A. Mahmood), jingsun@mail.sic.ac.cn (J. Sun).

https://doi.org/10.1016/j.jhazmat.2020.123402
Received 9 June 2020; Accepted 2 July 2020
Available online 08 July 2020

1. Introduction

Volatile organic compounds (VOCs) in the indoor air can be harmful, and some may be toxic, mutagenic, and teratogenic (Suárez et al., 2019). The presence of VOCs is accounted for the increasing ozone content in the atmosphere as well as the photochemical smog formation. Different types of VOCs, i.e., acetaldehyde, formaldehyde, benzene, toluene, and xylene are constantly delivered into the environment through different natural and anthropogenic sources (Broday et al., 2020; Zheng et al., 2019). Therefore, it is important to eliminate VOCs from both the indoor and the outdoor environments. Several procedures have been adopted for the VOCs abatement, which include, non-thermal plasma (Mustafa et al., 2018), adsorption on carbon materials (Zhang et al., 2017), biological treatment (Munoz et al., 2013), electro-catalytic method (Lee et al., 2020), adsorption by porous materials (Zhu et al., 2020), and photocatalytic oxidation (Li et al., 2017a,b, Wang et al., 2009). Among these, the photocatalytic oxidation (PCO) is regarded as a promising technique for the removal of VOCs (Ji et al., 2017; Weon et al., 2017). For example, the deactivation of adsorbent used in the adsorption process lowers their efficiency (Zou et al., 2019). Also, during the thermal catalytic decomposition, a high temperature (> 700℃) is required for the complete elimination of VOCs, which is not feasible for the low VOCs content (Jones et al., 2014). In contrast, oxide-based semiconductor materials such as TiO_2 can be used to harvest solar light to efficiently eliminate VOCs under light illumination (Petronella et al., 2017).

Titanium dioxide (TiO_2) is among the most studied semiconductor materials for the photocatalytic as well as energy applications (Naldoni et al., 2019; Tofighi et al., 2019). Additionally, TiO_2 has been thoroughly considered for the removal of organic pollutants owing to its outstanding oxidizing properties, abundance, and nontoxicity (Nie et al., 2018; Rao et al., 2019). However, as TiO_2 is a wide bandgap ($E_g = \sim 3.2$ eV) semiconductor material, thus, it can only harness light in the ultraviolet (UV) region, which constitute < 5% of the solar spectrum. Another issue, which further limits the usefulness of TiO_2 is the fast recombination of the photoinduced hole-electron pairs (Shen et al., 2019). To overcome these issue, different strategies have been adopted, which include precious metal deposition, development of heterojunctions, and doping of foreign elements in the TiO_2 crystal (Bai et al., 2019; Pradhan and Uyar, 2019; Zhou et al., 2019). For instance, the effect of commercially available TiO_2 microstructures has been studied for the removal of toluene, acetone, and acetaldehyde (Bianchi et al., 2014). It has been reported that efficient adsorption of the pollutant gas molecules on the surface plays a key role in the subsequent photodegradation reaction. The FTIR study suggested that the surface Ti−-OH-T−i bridge due to the OH groups on TiO_2 surface play a significant role for the efficient photodegradation. The larger number of Ti−OHT−i bridged species were found to facilitate the photodegradation of acetone and acetaldehyde. Among the various types of TiO_2 samples, commercial TiO_2 (PC105; $E_g = 3.19$ eV) demonstrated a high photocatalytic activity for the photodegradation of acetone and acetaldehyde, when compared with the other nano- and micro-sized TiO_2 powders, i.e., P25 (3.21 eV), 1077 (3.15 eV), and AT-1 (3.15 eV). Furthermore, the toluene photodegradation resulted in some irreversible changes on the photocatalyst surface. It was noticed that Ti−OH sites disappeared during the photodegradation of toluene, which resulted in an incomplete removal of toluene even after a prolonged reaction time (6 h). In another study, TiO_2 nanoparticles were incorporated into a metal-organic framework (MOF), NH_2-UiO-66, where the concentration and morphology of TiO_2 particles were controlled using the hard-soft acid-base (HSAB) principle (Yao et al., 2018). In contrast to pure TiO_2, TiO_2/NH_2-UiO-66 composites demonstrated a high photocatalytic activity for VOCs, which was attributed to an efficient charge separation due to a good interfacial contact between TiO_2 and MOF. Moreover, the photodegradation of styrene was substantially improved under the visible light illumination. High conversion efficiency of 99 % was recorded for the 5%wtTiO_2@NH_2-UiO-66 composite in contrast to pure TiO_2 (32 %).

The surface modification of TiO_2 has been given a considerable interest. For example, Pt and F-modified TiO_2 has shown excellent photocatalytic efficiency for the indoor air pollutant (Weon et al., 2018). The Pt/TiO_2 exhibited a high photocatalytic response for toluene photodegradation, however, showed deactivation during the repetitive tests. In contrast, the F-TiO_2 was more stable, but initial efficiency was almost similar to bare TiO_2. However, when the F-TiO_2/Pt system was tested for toluene, it demonstrated an excellent photodegradation efficiency and stability. The surface fluorination facilitated more stable mobile O˙H radicals by replacing surface O˙H-groups. While the Pt-species on the surface inhibited the electron-hole recombination and promoted the hole transfer to the adsorbed water molecules. The mobile O˙H species obstructed the absorption of carbonaceous intermediate species on the surface, which prolonged the activity of the catalyst. Although, significant improvements have been achieved in TiO_2 based photocatalysts for the removal of VOCs, the topic is still actively pursued in the literature. The main issues, which are to be solved is the replacement of precious metals as cocatalysts to lower the device cost, while improving the charge separation and light harvesting capabilities.

Currently, a new class of “zero-dimensional” nanostructures i.e., carbon quantum dots (CQDs), are gaining much attention to sensitize TiO_2 (Jing et al., 2019). CQDs are categorized as quasi-spherical nanoparticles (NPs) with an average diameter of less than 10 nm (Di et al., 2015). Their structure is amorphous or crystalline, containing carbon rings with sp^2 carbon clusters or they may appear as diamond-like rings comprised of sp carbon. Due to the synergistic effect, the decoration of CQDs on TiO_2 not only suppresses the charge recombination process in TiO_2, but also improves the light absorption capacity (Liang et al., 2019). Lately, CQDs modified semiconductor materials have been studied for various photocatalytic and electrical applications, for example, CQDs/BiOI (Di et al., 2016), CQDs/$ZnFe_2O_4$ (Huang et al., 2017), CQDs/$CaTiO_3$ (Wang et al., 2018), CQDs/CuO (Ma et al., 2016), and CQDs/TiO_2 (Li et al., 2017a,b). The photodegradation of VOCs using CQDs/TiO_2 has been rarely studied. One such attempt has been recently reported by our group (Hu et al., 2018). Our group used CQDs/TiO_2 composites to photodegrade gaseous acetaldehyde. The results showed that with 3 wt% CQDs/TiO_2, 99 % of acetaldehyde (500 ppm) could be photodegraded when compared with pristine TiO_2 (46 %) with a flow rate of 20 standard cubic centimeters per minute (sccm). Additionally, 3%wt CQDs/TiO_2 exhibited a substantial conversion efficiency (30 %) under visible light irradiation. These outcomes are promising and led us to examine CQDs and TiO_2 composites for other VOCs.

Herein, CQDs modified TiO_2 nanocomposites were synthesized, showing an outstanding degradation efficiency under UV–vis light for the mixed VOCs, which include benzene, p-xylene, and toluene. TiO_2 nanoparticles were decorated with different wt% of CQDs and investigated their photocatalytic activity within the UV and visible region. The effect of CQDs on the absorptivity of pollutant gas molecules, optical properties, and degradation of mixed VOCs under light irradiation was studied in detail. The adsorption behavior of pollutant gas molecules was also investigated using periodic density functional theory (DFT). Additionally, the origin of enhanced photocatalytic activity was rationalized by investigating the electronic structure of the CQDs and TiO_2 interface, using DFT. Our study explores the potential use of CQDs and TiO_2 nanocomposites to remove mixed-VOCs for the first time, which will be of high significance for the future studies.

2. Experimental section

2.1. Synthesis of pure TiO_2

Two different synthesis routes were adopted to synthesize pure TiO_2 and CQDs, which include hydrothermal method (Chen et al., 2018) and

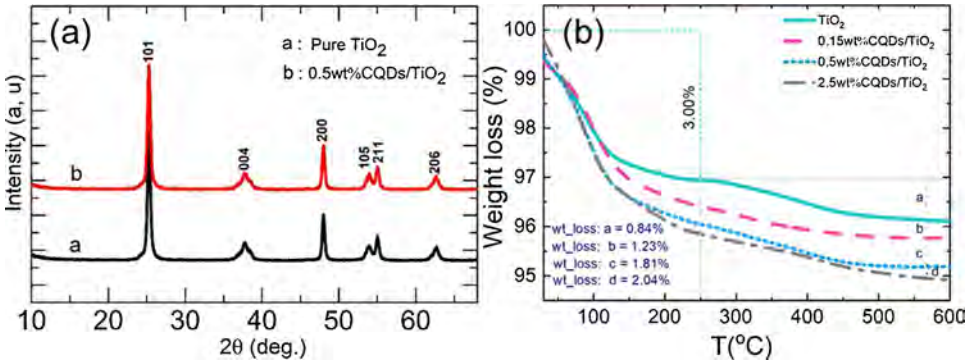

Fig. 1. X-ray diffraction (a) and thermogravimetric analysis (b) of the pure and *x*wt%CQDs/TiO_2.

citrate precursor method, respectively. At first, we synthesized TiO_2 NPs with desired dominant facets. For this purpose, titanium butoxide ($C_{16}H_{36}O_4Ti$; 97 %; Sigma-Aldrich) and hydrogen fluoride (HF: 40 %; Sigma-Aldrich) were mixed in a dry Teflon vessel, which was heat-treated in an electric furnace at 200℃ for 24 h. The product precipitates were collected through centrifugation (10,000 rpm) for 10 min and thoroughly washed with deionized water. To remove the surface fluoride ions, as-prepared TiO_2 NPs were sonicated for 1 h in 0.1 M NaOH and kept at room temperature for 24 h, which were eventually washed with deionized water and dried in an electric furnace at 100℃.

2.2. Synthesis of carbon quantum dots

The citric acid decomposition method was adopted to synthesize water soluble CQDs (Martindale et al., 2015). In a typical reaction, 40 g of citric acid was put through 180℃ for 40 h in an electric furnace. The resulting brown gelatinous matter was carefully dissolved in 5 M NaOH solution and the pH was adjusted as 7. Finally, we used freeze drying procedure to achieve the CQDs powder.

2.3. Composites preparation

To start with, 1 g of TiO_2 was dispersed in a mixture solution containing 5 mL deionized water and 15 mL absolute ethanol, which contained 0.5 wt% CQDs. This solution was first stirred for 12 h on a magnetic hot plate at room temperature and eventually dried at 70℃ under constant stirring. The dried powder was calcined in the range from 100 to 300℃. Our results showed that 200℃ is the best calcination temperature, which revealed superior photocatalytic activity compared to other samples, hence the other compositions were also calcined at this temperature. Different wt% of CQDs were used to synthesize 0.15, 0.5, and 2.5 wt% CQDs decorated TiO_2 NPs.

2.4. Characterization

The X-ray diffraction (XRD) profiles were collected using Ultima IV 2036E102, Rigaku Corporation, Japan X-ray diffractometer with Cu $K_{\alpha 1}$, (1.54 Å) source. Particle morphology and elemental analysis was carried out using a field emission scanning electron microscope (FESEM: JEOL JSM-6700 F) coupled with an EDS. High resolution transmission electron microscope (HRTEM: JEOL 2100) was used for an in-depth nanostructure analysis, operating at 200 kV coupled with LaB6 source. Optical characterization was carried out using a model Perkin Elmer Lambda 950 UV–vis-NIR absorption spectrometer and Edinburg FL/FS900 photoluminescence spectrophotometer using λ_{Exc} = 320 nm. The surface chemical states were identified through XPS (Thermo scientific ESCALAB 250Xi) analysis. The Brunner- Emmett -Teller (BET) specific surface area of the samples was analyzed using a nitrogen desorption isotherm apparatus (Micrometrics ASAP 3000). A model ESR (JES-FA200) spectrometer was used to study the production of oxide radicals. The computational detail is given in supplementary section S1.

2.5. Photocatalytic test

The sample powders (0.1 g) were coated on a glass substrate prior to the photodegradation reaction. The as-prepared photocatalysts were transferred to an automated flow reaction chamber with a coupled GC (Fig. S1). The adsorption-desorption process was monitored to achieve an equilibrium, which were subsequently irradiated using UV–vis light. Fresh samples have been used for every test except for the cyclic experiment. The test was also carried out without a catalyst (empty reaction chamber) for comparison. In the beginning, the instrument was stabilized under flow of the gas-phase mixed-VOCs (60 ppm), which was eventually allowed to flow in the reaction chamber under the dark condition. The photodegradation was monitored through GC under light illumination. The reading was automatically recorded in 10 min time intervals. The flow rate was kept constant as 20 sccm.

3. Results and discussion

3.1. X-ray diffraction and thermal analysis

Fig. 1a shows the XRD results of pure and CQDs (0.5 wt%) modified TiO_2 NPs. The XRD results confirmed the formation of single phase anatase TiO_2, which matched well with the standard PDF no: 21-1272. No impurity peaks could be seen in the XRD results. The CQDs decoration did not affect the XRD peaks profile, which suggested that CQDs on the surface would not affect the crystal lattice of TiO_2. The lattice parameters of pure TiO_2 were calculated as $a = b = 3.7897$ Å, $c = 9.5214$ Å, which agreed well with the previous reports (Challagulla et al., 2017). The lattice parameters of 0.5 wt%CQDs/TiO_2 nanocomposite were $a = b = 3.7904$ Å, and $c = 9.5325$ Å, which displayed no considerable difference. The XRD peak profile of pure CQDs revealed a broad hump around $2\theta = 29.8^{\circ}$ (Fig. S2), which was attributed to the lattice spacing 3 Å, much like (200) reflection (d_{002} = 3.4 Å). Somewhat similar results have been previously observed in a disordered graphitic-like structure (Peng and Travas-Sejdic, 2009). We further used thermogravimetric (TG) analysis to estimate the amount of CQDs on TiO_2 NPs (Fig. 1b). The weight-loss below 200 °C was attributed to the removal of adsorbed water, which accounts for only 3% in the case of pure TiO_2 (Ramimoghadam et al., 2014). The corresponding weight-loss in this region increased by changing the wt% of CQDs, which can be inferred as that the adsorption of water was facilitated in the presence of CQDs. The weight-loss beyond this region was attributed to the surface adsorbed moisture, OH species, residual organics, and the combustion of CQDs. The CQDs decorated TiO_2 NPs showed a high weight-loss, which suggested that more combustion products were released due to the presence of CQDs on TiO_2 NPs. The corresponding wt % losses for the pure and 0.15, 0.5, and 2.5 wt%CQDs decorated TiO_2

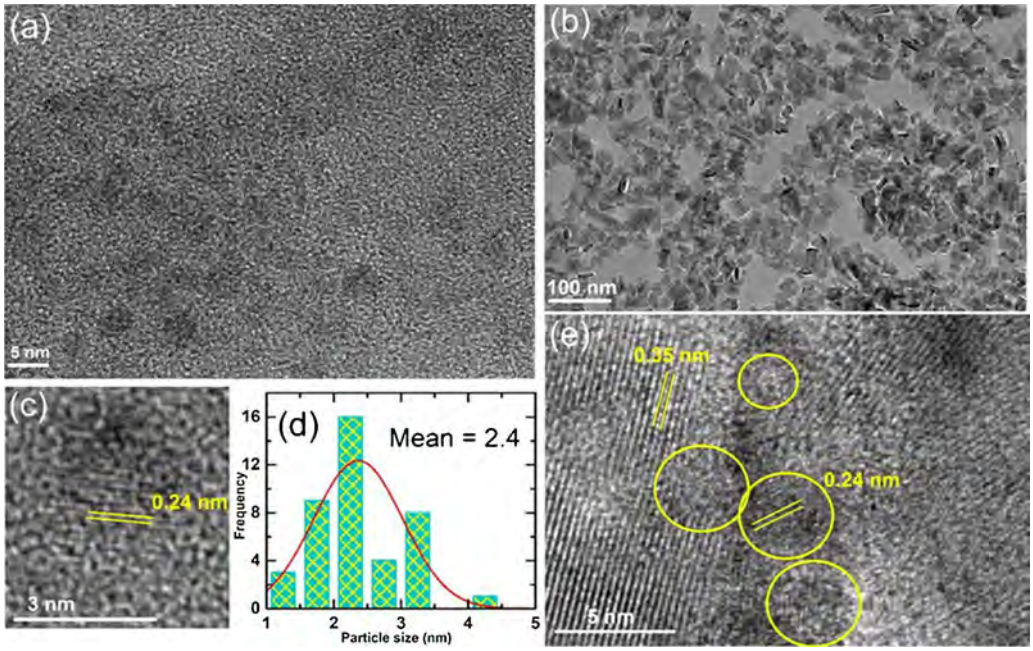

Fig. 2. TEM and HRTEM micrographs of CQDs and 0.5 wt%CQDs/TiO_2; (a) TEM of CQDs, (b) TEM of 0.5 wt%CQDs/TiO_2, (c) HRTEM of CQDs, (d) particle size distribution of CQDs, (e) HRTEM of 0.5 wt%CQDs/TiO_2.

were calculated as 0.84 %, 1.23 %, 1.81 %, 2.04 %, respectively. The TG analysis confirmed the presence of CQDs on TiO_2 NPs. Also, the variation in wt% indicated that the content of CQDs was successfully varied in our experiment.

3.2. Microstructure analysis

The TEM and HRTEM images are given in Fig. 2. Pure CQDs revealed a homogeneous spherical particle morphology with varying particle size (Fig. 2a). The average particle size was calculated as 2.4 nm using particle size distribution method (Fig. 2d). The HRTEM image displayed the characteristic graphitic and amorphous carbon regions (Fig. 2c). The average distance among the lattice fringes of the graphitic area is calculated as 0.24 nm, which is equivalent to (100) interlayer spacing (Baker and Baker, 2010). The FESEM micrographs and EDS analysis of pure and 0.5 wt%CQDs/TiO_2 revealed a cube-like morphology, which is a characteristic growth habit of TiO_2 NPs along the < 001 > direction (Fig. S3) (Wang et al., 2020). The mean particle size was calculated as 62.1 nm using particle size distribution method (Fig. S4). The EDS study confirmed the presence of titanium, oxygen, and carbon, while the wt% ratio of C (2.13 %) was marginally higher in the 0.5 wt%CQDs/TiO_2 than pristine TiO_2 (1.94 %). Additionally, Fig. 2b verified the cuboidal disk morphology of TiO_2 NPs. The HRTEM confirmed the successful deposition of CQDs on TiO_2 surface (Fig. 2e). The interplanar distance was measured as 0.35 nm, which was attributed to (101) plane of anatase TiO_2 (Li et al., 2018; Yang et al., 2018). The lattice distance of CQDs is 0.24 nm and the lattice planes for TiO_2 and CQDs can be noticed in the same region. These results further confirmed the successful decoration of CQDs on TiO_2 NPs.

3.3. X-ray photoelectron study

Fig. 3 shows the XPS analysis of CQDs modified TiO_2. The survey XPS profile exhibited the key constituent elements (Fig. 3a). The raw data was analyzed using Gaussian-fit to highlight the hidden peaks in the XPS pattern. Three peaks were identified in the C 1s spectrum, which occurred at the binding energies (B.E), such as, 285.8 eV, 287.3 eV, and 289.2 eV. These peaks were attributed to C═C, CH, and OCO−−═, respectively (Shi et al., 2017; Wang et al., 2019). In the case of O 1s, three peaks were identified at B.E 530.8 eV, 531.4 eV, and 532.5 eV, which were attributed to lattice oxygen, oxygen bound to reduce Ti^{3+} state forming Ti_2O_3, and O-H, respectively. The Ti 2p peak was resolved into four distinguished peaks (Fig. 3d). Similar peaks have been previously reported for the cobalt doped TiO_2 systems (Bharti et al., 2016). The high intensity peaks around the B.E 459.4 eV and 465.2 eV were associated with the $Ti^{4+}2p_{3/2}$. The peaks at B.E 457.8 eV and 460.9 eV were attributed to the presence of Ti^{3+} $2p_{1/2}$. The presence of Ti_2O_3 can be evidenced from the Ti^{3+} $2p_{1/2}$ and 531.4 eV peak in O 1s. It has been reported previously that CQDs might reduce Ti^{4+} to Ti^{3+} (Lin et al., 2018). The shifting of Ti 2p peaks of CQDs decorated TiO_2 sample in contrast to pure TiO_2 suggested a strong interaction between the CQDs and TiO_2 NPs, which might have influenced the surface states of TiO_2.

3.4. Specific surface area, light absorption, and photoluminescence studies

The BET surface area of pure and *x*wt%CQDs/TiO_2 nanocomposites were measured using the nitrogen-adsorption isotherm. The results are shown in Fig. 4a, and b. No significant difference was observed among the pure and CQDs modified TiO_2 NPs. The corresponding specific surface area and average pore diameter of pure TiO_2 were determined as 89.92 m^2/g and 20.49 nm. The specific surface area values of the CQDs modified TiO_2 were 90.03, 90.74, and 90.89 m^2/g corresponding to 0.15, 0.5, and 2.5 wt% of CQDs modified TiO_2 NPs. The average pore diameter of CQDs modified TiO_2 was 16.50, 16.00, 17.21 nm, respectively. The UV–vis absorption spectrum (Fig. 4c) demonstrated a non-linear redshift with the increasing CQDs content. For example, the absorption edge of 0.5 wt%CQDs/TiO_2 nanocomposite shifted more in contrast to pure and other CQDs modified samples. This behavior could be due to the surface sensitization of TiO_2 NPs after CQDs decoration, which improved the light absorption capability. The bandgap values were calculated from the UV–vis spectra using equation $E = hc/\lambda$.. Where h (6.626×10^{-34} Joule sec) is the Plank constant, c (3.0×10^8 meters/sec) is the speed of light, and λ is the cutoff wavelength. The cutoff wavelength for the pure and CQDs modified TiO_2 samples were determined from the corresponding UV–vis spectrum. The bandgap values of pure and 0.15, 0.5, and 2.5 wt%CQDs/TiO_2 nanocomposites were calculated as 3.18, 3.15, 3.12, and 3.14 eV, respectively. The

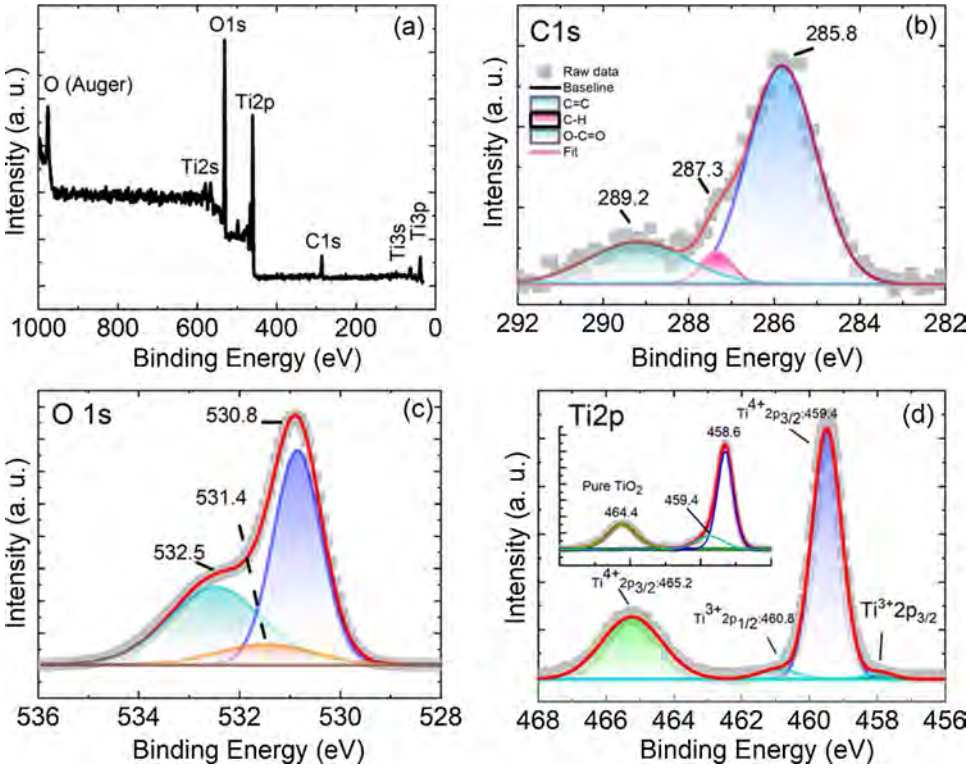

Fig. 3. XPS spectra of 0.5 wt%CQDs/TiO_2, (a) XPS survey spectra, (b) C1 s, (c) O1 s, (d) Ti2p.

schematic bandgap diagram is also given in Fig. 4e. The PL results are given in Fig. 4d. The PL spectra exhibited a broad peak around the 400 nm, which is due to the band-band photoluminescence phenomenon (Etacheri et al., 2010). A significant decrease in the PL intensity was observed for the CQDs decorated TiO_2 nanocomposites. For example, the 0.5 wt%CQDs/TiO_2 nanocomposite demonstrated the lowest peak intensity in this region, in contrast to pure TiO_2 and other CQDs modified samples. This behavior could be associated with the improved charge separation process due to the presence of CQDs on TiO_2 NPs. It has been well thought out that the photoinduced electrons excited in pure TiO_2 recombine in a short time, which affects the photocatalytic performance of pure TiO_2. Once the CQDs are decorated on TiO_2 surface, the photoexcited electrons can further conduct in the CQDs structure, which improves the charge separation efficiency (Wang et al., 2019).

3.5. Adsorption and photodegradation study

The photocatalytic activities of the pure and CQDs decorated TiO_2 NPs were studied using gas-phase mixed VOCs as the sample pollutant gas, which included benzene (20 ppm), p-xylene (20 ppm), and toluene (20 ppm). The adsorption-desorption equilibrium was achieved in the dark prior to the photodegradation process under UV–vis light illumination. The mixed VOCs was allowed to flow in the reaction chamber with a flow rate of 20 sccm. The results are shown in Fig. 5. The curve area of the empty chamber was deducted from the catalyst area to determine the %increase in adsorption. Fig. 5a and b shows the adsorption curves and (%)adsorption, respectively. When pure TiO_2 was used as the photocatalyst in the reaction chamber, a substantial increase in the adsorption area was observed, which suggested that pure TiO_2 adsorbed the gas molecules. Pure TiO_2 showed a 20 % rise in the adsorption of mixed VOCs in contrast to the empty reaction chamber. The CQDs (0.5 wt%) decorated TiO_2 NPs further improved the adsorption of mixed VOCs. The 05 wt%CQDs decorated TiO_2 NPs were calcined at different temperature and the photocatalytic activities of the as-prepared samples were tested to optimize the nanocomposite fabrication process. The calcination temperature improved the adsorption capacity of the 0.5 wt%CQDs decorated TiO_2 nanocomposite. The sample calcined at 300°C exhibited a 99 % rise in adsorption when compared with the blank chamber. The photodegradation test was performed after achieving the dynamic adsorption-desorption equilibrium. The empty chamber did not show any photocatalytic response (Fig. 5c). When TiO_2 NPs were utilized as the photocatalyst, a high photodegradation efficiency (44 %) was achieved (Fig. 5d). Next, it had been observed that the calcination temperature for decorating the CQDs on TiO_2 NPs affected the photocatalytic activities. For example, the sample calcined at 200 °C demonstrated a higher photodegradation efficiency (64 %) than pure TiO_2 as well as the other CQDs/TiO_2 nanocomposites. The sample calcined at 250°C exhibited a 53 % photodegradation efficiency, which was still higher than pure TiO_2. However, the CQDs/TiO_2 calcined at 100°C (42 %) and 300 °C (25 %) showed a poor performance than pure TiO_2. Hence, it can be inferred that 200°C is an optimum calcination temperature to prepare CQDs and TiO_2 nanocomposites, which demonstrated relatively good adsorption and excellent photocatalytic activity than pure TiO_2.

Fig. 6 shows the photodegradation of mixed-VOCs, including benzene, p-xylene and toluene, on pure and *x*wt%CQDs/TiO_2 (x = 0.15, 0.5, 2.5) nanocomposites. The corresponding photodegradation efficiency is shown in Fig. 6e. The average photodegradation efficiency is given in Fig. S5. When pure TiO_2 was used as the photocatalyst in the reaction chamber, 44 % of the mixed VOCs were degraded under UV–vis light illumination (Fig. S5b). The individual analysis of benzene, p-xylene, and toluene showed a significant difference (Fig. 6a). For example, pure TiO_2 only photodegraded 4 % of benzene. In contrast, 42 % of p-xylene and 82 % of toluene were photodegraded. The CQDs decoration improved the overall photodegradation efficiency of TiO_2 NPs. In any case, only a small amount of benzene is photodegraded, while a high photodegradation efficiency is achieved in the case of toluene. The sample 0.15 wt%CQDs/TiO_2 did not display any photodegradation activity for benzene. The ease of photodegradation order

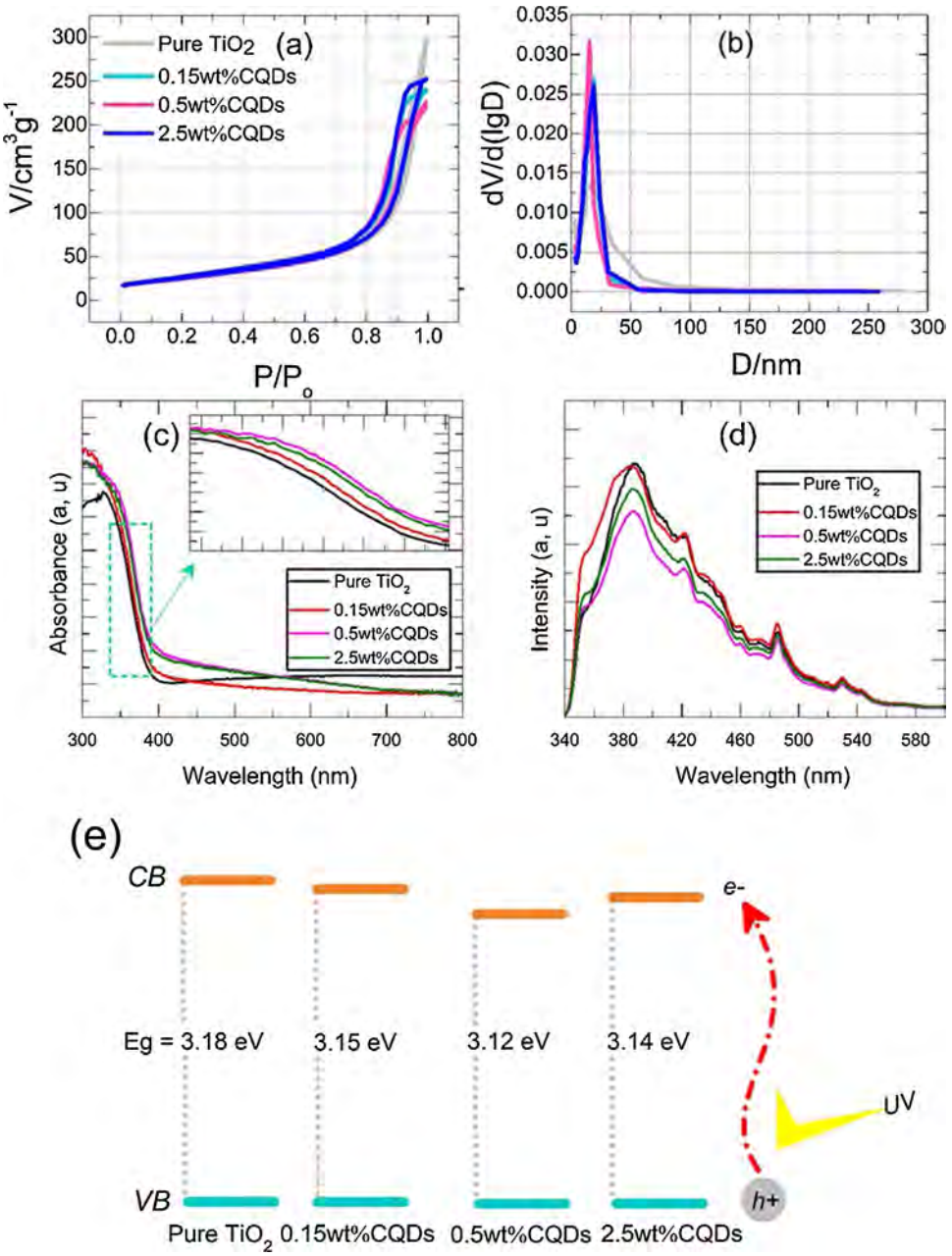

Fig. 4. BET surface area analysis, which include nitrogen adsorption isotherm and pore diameter (a-b), optical absorption (c), PL spectra (d). The schematic band diagram is also given (e).

for various VOCs photodegraded in this work is arranged as: toluene > p-xylene > benzene. The sample 0.5 wt%CQDs/TiO_2 showed an excellent overall performance. The average photodegradation efficiency for the mixed gases was recorded as 44 %, 54 %, 64 %, and 51 %, corresponding to pure TiO_2 and 0.15, 0.05, 2.5 wt%CQDs/TiO_2, respectively (Fig. S5b). The sample 0.5 wt%CQDs/TiO_2 showed 31 %, 64 %, and 99 % photodegradation efficiency in the case of benzene, p-xylene, and toluene, respectively (Fig. 6c). Therefore, 0.5 wt%CQDs/TiO_2 nanocomposite is the best photocatalyst in this work, which exhibited superior photocatalytic activity. Besides, we compared the overall photodegradation behavior within the visible region of pure and 0.5 wt%CQDs/TiO_2 (Fig. S6). Pure TiO_2 did not show any photocatalytic activity beyond 400 nm, which is quite predictable; while, the sample 0.5 wt%CQDs/TiO_2 demonstrated a considerable photocatalytic efficiency (13 %) within the visible region. It has been reported that the degradation of VOCs mixture exhibits a different behavior in contrast to isolated mode. For example, the presence of trichloroethylene (TCE) (225 − 753 mg/m^3) were found to improve the photodegradation of toluene on anatase TiO_2 under UV-light illumination to achieve 90–100 % degradation (Luo and Ollis, 1996). The variation in toluene concentration below ~90 mg/m^3 deteriorated the TCE degradation. Also, pure TiO_2 demonstrated deactivation during the PCO of toluene despite the presence or absence of TCE. Similar behavior was observed when dilute mixture of toluene (10 − 750 mg//m^3) and perchloroethylene (PCE) and 1,1,3-trichloropropene (TCP) were used, which eventually increased the toluene conversion (100 %) (Michael L. Sauer et al., 1995). However, the commercial TiO_2 (Degussa P25) showed deactivation during the photodegradation reaction. Thus, in our study the mixture effect could possibly influence the overall degradation mechanism. The cyclic stability test of the 0.5 wt%CQDs/TiO_2 nanocomposite is also perfumed (Fig. 7). Interestingly, no considerable deterioration in the photocatalytic performance is noticed under five

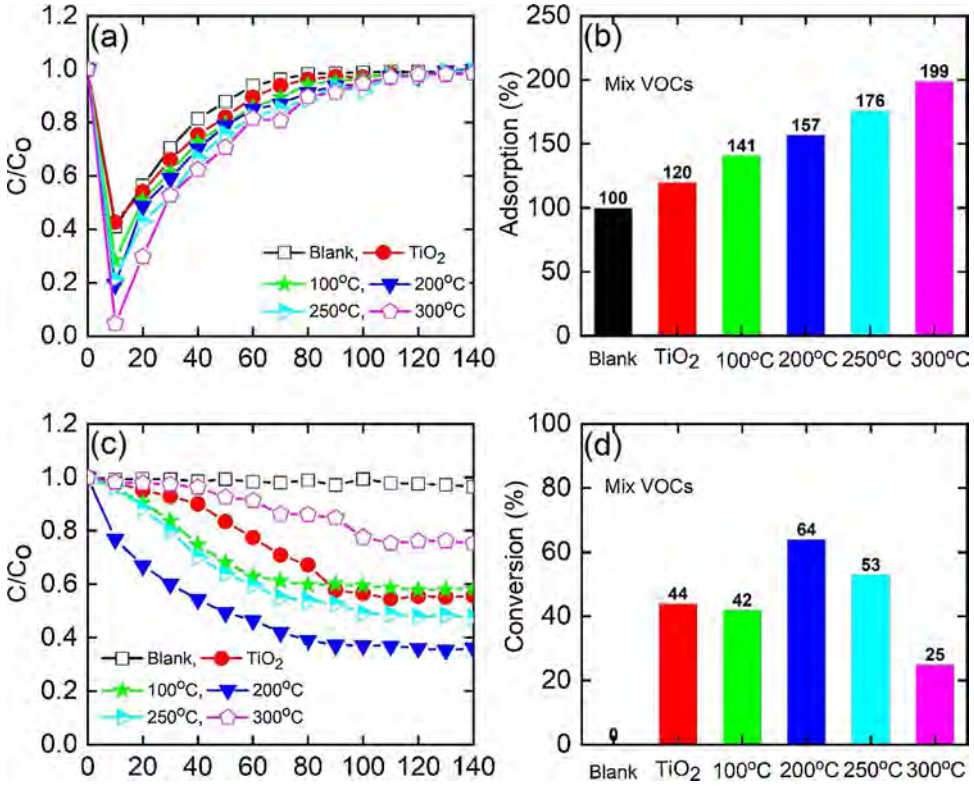

Fig. 5. (a) Adsorption, (b) percent adsorption, (c) photodegradation, and (d) conversion efficiency of mixed-VOCs in the presence and absence of photocatalysts. The temperature corresponds to the calcination temperature of the 0.5 wt%CQDs/TiO_2 composites.

repeating cycles, which is useful for the pragmatic device applications. In a previous attempt, the photodegradation of n-hexane, n-butyl acetate and toluene mixture on TiO_2 suggested that toluene deactivated the photocatalysts, while showed a poor photodegradation (Moulis and Krýsa, 2013). Thus CQDs improved the stability of TiO_2 NPs in our study. The ESR experiment was carried out to investigate $^{\cdot}OH$ and $O_2^{\cdot-}$ radical's production (Fig. 8). The results showed sharp peaks for the $O^{\cdot}H$ radicals in the case of 0.5 wt%CQDs/TiO_2 nanocomposite while pristine TiO_2 exhibited sharp peaks for the $O_2^{\cdot-}$ radicals. These two reactive radicals are crucial for driving a surface catalyzed reaction. Therefore, the 0.5 wt%CQDs/TiO_2 nanocomposite could be more active in the photodegradation steps, which involves the $O^{\cdot}H$ radicals, since large number of $O^{\cdot}H$ radicals will be available in the case of CQDs/TiO_2 nanocomposites. As mentioned previously regarding the distinct role of TiO_2 {001}(Fu et al., 2019) facets for the hole migration phenomenon, more $O^{\cdot}H$ radicals were anticipated in our study. Additionally, CQDs can trap some electrons in defective graphene like structure, which would have increase the $O^{\cdot}H$ radical's production.

Because of the distinctive molecular structure of different VOCs photodegraded in this experiment, it was anticipated that these VOCs

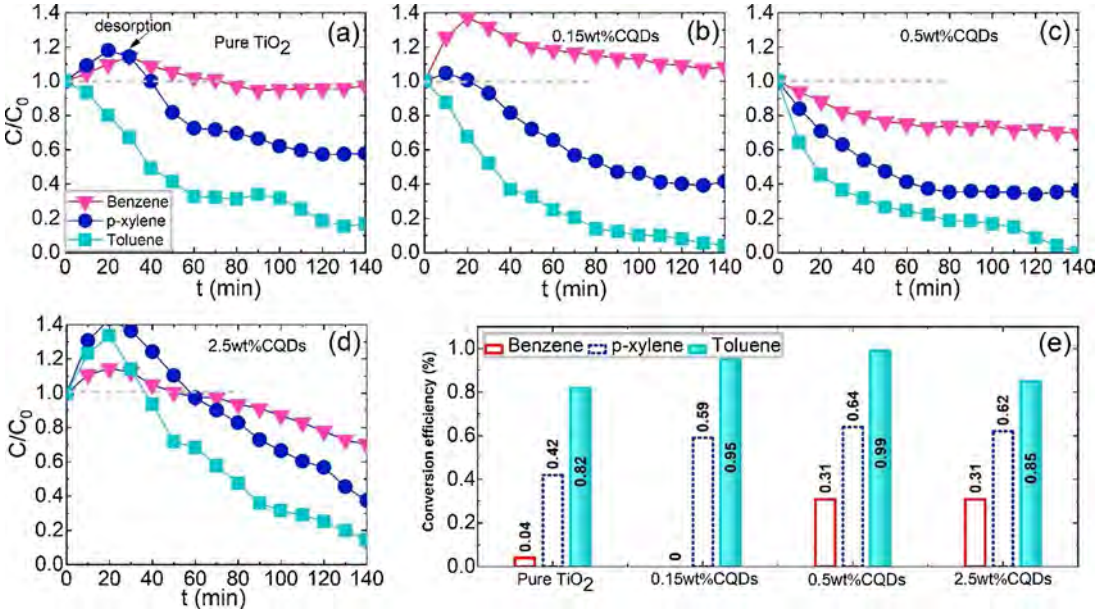

Fig. 6. Photocatalytic degradation of mixed-VOCs and the corresponding conversion efficiencies.

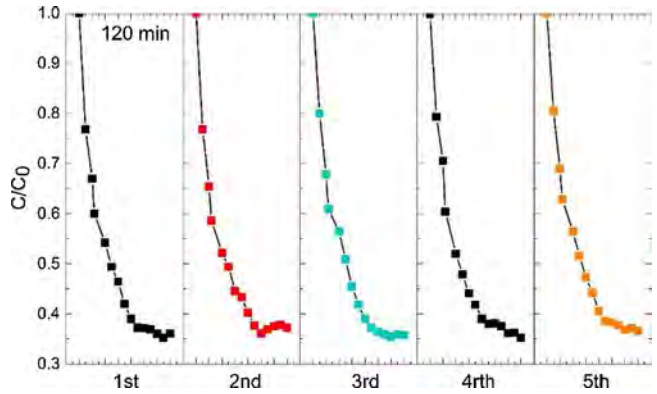

Fig. 7. Cyclic test for the photodegradation of mixed-VOCs on 0.5 wt%CQDs modified TiO_2 NPs.

(benzene, toluene, and p-xylene) will demonstrate a unique affinity towards the TiO_2 surface. For example, a similar behavior was observed during the photodegradation of propanol, propanal, propanone, propene, and propane mixture (Zorn et al., 2010). A detailed multi-component experiments suggested that those compounds, which exhibit stronger binding energy on the catalyst surface will replace weakly bonded pollutant gas molecules, which will affect their phootoconversion, until the strongly bonded gas molecules are oxidized to a low level. Also, the competition kinetics among the different gas molecules might be responsible for their distinctive degradation behavior in the mixture. Such a behavior was observed in the case of p-xylene, toluene, and acetone mixture degradation on TiO_2 (Liang et al., 2010). The by-product of p-xylene and acetone promoted the degradation of toluene. The adsorption of toluene was higher on the catalyst's surface, which were attributed to the unsymmetrical structure of toluene, in contrast to p-xylene and acetone. The mixture-effect to delay the photodegradation of VOCs has also been observed recently for the toluene, decane, trichlorethylen mixture (Debono et al., 2017). Since the XRD results showed the polycrystalline nature of TiO_2 NPs, even so, TiO_2 {001} facets are more reactive contrasted to TiO_2 {101} facets. Therefore, only TiO_2 (001) surface was used to compute the adsorption energy of benzene, p-xylene, and toluene using DFT calculations. The fully relaxed structures of benzene, p-xylene, and toluene are shown in Fig. S7. Benzene, p-xylene, and toluene were allowed to relax on TiO_2 (001) surface (Fig. S8). The optimized configurations of the molecules exhibited a position where the aromatic rings are parallel to TiO_2 (001) surface. The adsorption of molecules extended the Ti_{5c}-O_{2c} bond distance on the surface. When it comes to benzene, this bond length was 1.73 Å. Regarding p-xylene and toluene, this bond distance was measured as 1.74 Å and 1.75 Å, respectively. Hence, it can be inferred that toluene showed a strong surface affinity in contrast to benzene and p-xylene. The corresponding adsorption energy (E_{ads}) values for benzene, p-xylene, and toluene are calculated as 0.212, 0.362, and 0.410 eV, respectively. These values further verified the strong interaction of toluene with TiO_2 (001) surface than benzene and p-xylene. The electron density difference results are given in Fig. S9. The gray region represents the electron-rich region, while the green region shows the electron depleting region. The electron density difference (EDD) results showed a high electron density around the aromatic ring. Therefore, it can be concluded that the benzene ring containing VOCs preferably adsorbs on TiO_2 (001) surface using π electrons of the aromatic ring and position parallel to the surface.

3.6. Electronic structure of the carbon quantum dots/TiO_2 (001) interface

The geometrically optimized structures of pure TiO_2 (001) and CQDs/TiO_2 interfaces, and pure CQDs are given in Fig. 9. The Ti_{5c}-O_{2c} distance was measured as 1.937 Å for the fully relaxed TiO_2 (001) surface (Fig. 9a). A significant distortion both in the CQDs framework and TiO_2 (001) surface was observed when the CQDs layer structure was interfaced with the TiO_2 (001) surface. For a single layer CQDs adsorb on TiO_2 (001) (Fig. 9b), the Ti_{5c}-O_{2c} bond distance increased (2.233 Å) by 14.7 %. An exchange of hydrogen atom occurred between the CQDs and surface O_{2c}. It can be inferred that various functional groups attached to CQDs can boost the adsorption process of CQDs on TiO_2 NPs. The bond distance between the surface O_{2c} and H was measured as 1.0 Å, which is closer to the O—H bond distance of the water molecule (0.975 Å). The C—H bond distance was initially calculated as 1.25 Å in pure CQDs (Fig. 9d), which increased to 1.57 Å after adsorption. The interfacial distance between the CQDs layer and TiO_2 (001) surface was 3.1 Å, which is in agreement with the previous reports for the graphene-based structures on TiO_2 surfaces (Ferrighi et al., 2016; Gao et al., 2013). The E_{ads} for the first layer of CQDs was calculated as 0.92 eV, which suggested a strong chemical interaction between the TiO_2 (101) surface and CQDs layer. A double layer of CQDs was also used (Fig. 9c), to mimic the original layered structure of CQDs proposed in the literature (Lim et al., 2015). The lateral distance between the first and second layers was calculated as 3.35 Å, which matched well with the experimental distance between graphene layers (3.34 Å) (Abdol et al., 2019). The E_{ads} for the second layer is calculated as 1.11 eV. The partial density of states (PDOS) was calculated to understand the charge carrier migration paths. The PDOS of the pure CQDs showed that C 2p states contributed in the valence band (VB), while the O 2p states primarily contributed in the conduction band (CB) (Fig. S10). A strong hybridization around the Fermi level between the O and Cp states were observed, while similar behavior was noticed around in the lower CB. The PDOS of TiO_2 (001) surface showed O 2p and Ti 3d states contributing in the VB near the Fermi level (Fig. S11). A strong hybridization was observed between O 2p and Ti 3d in the VB between −5.4 and −3.1 eV. It is clear that Ti 3d states majorly

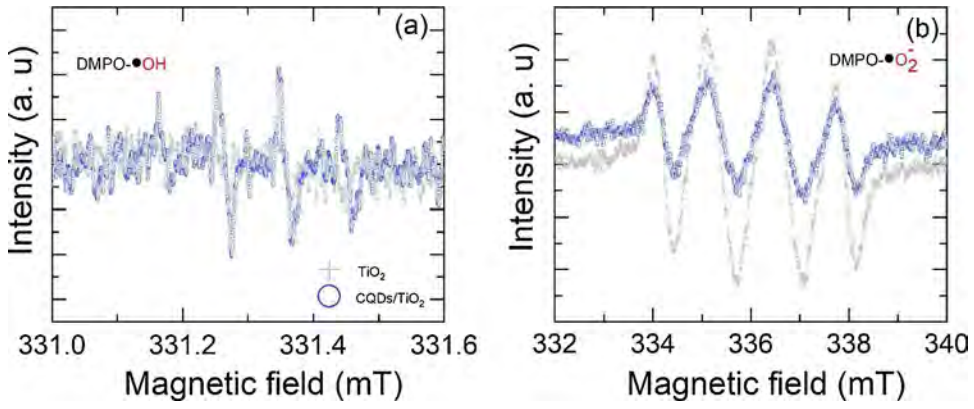

Fig. 8. Production of $^{\cdot}OH$ and $O_2^{\cdot-}$ radicals in the case of pristine and CQDs loaded TiO_2.

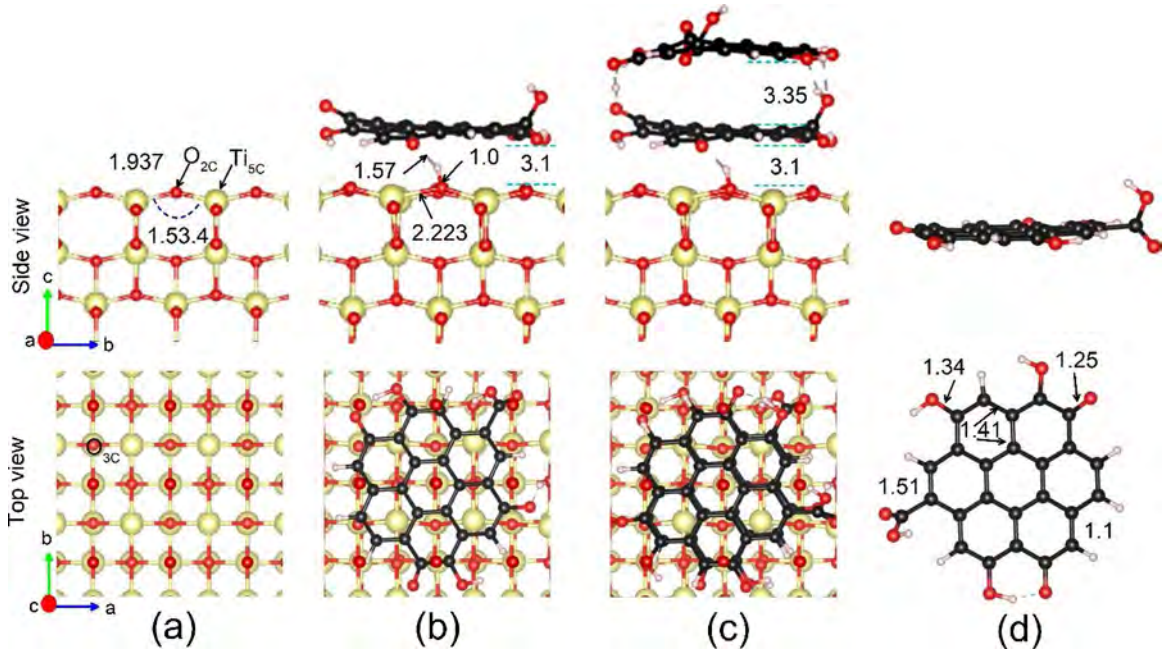

Fig. 9. Optimized structures of TiO_2 (001) surface, (b) single layer CQDs/TiO_2 (001) interface, (c) double layer CQDs/TiO_2 (001) interface, and (d) CQDs.

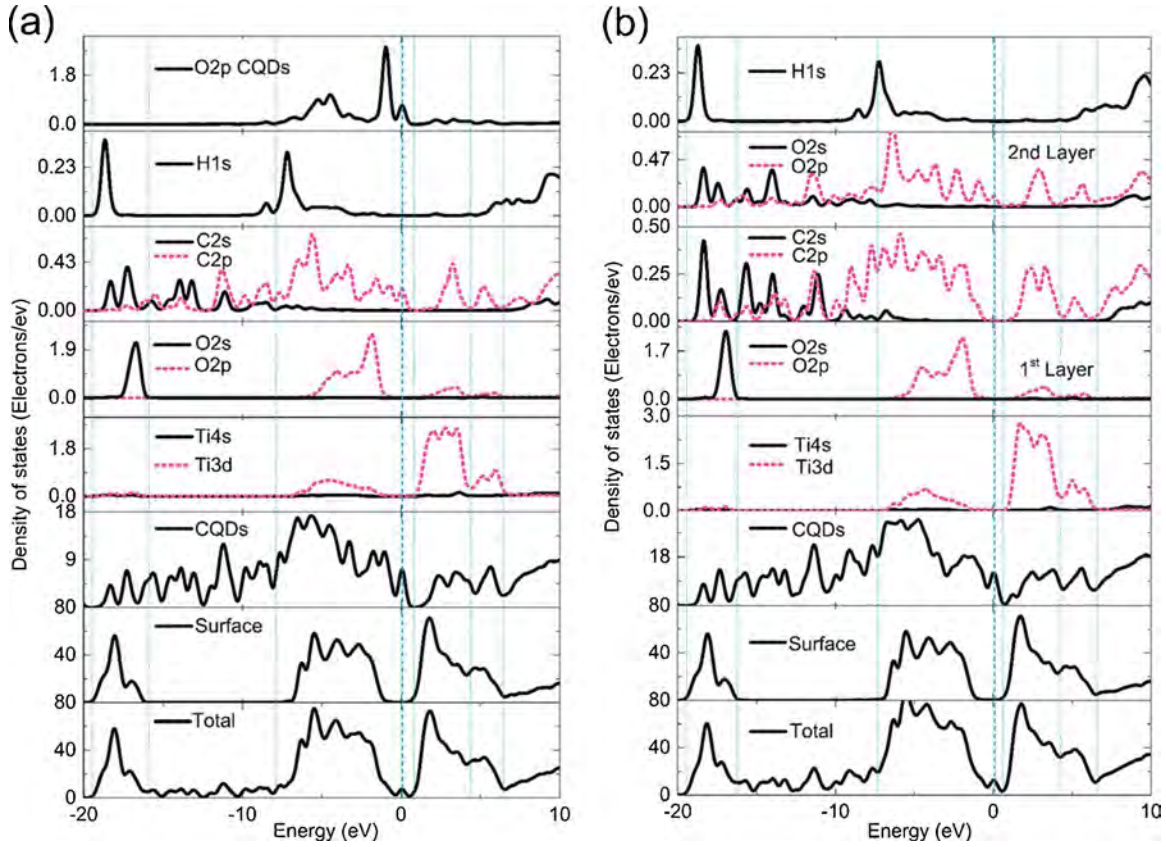

Fig. 10. PDOS (a) single layer CQDs/TiO_2 (001) interface and (b) double layer CQDs/TiO_2 (001) interface.

contributed in the lower CB and the O 2p states in the upper CB. Hence, it can be inferred that under light irradiation, the photoinduced electrons will transfer from the O 2p states to Ti 3d states. Fig. 10a and b shows the PDOS of the single and double layer CQDs on TiO_2 (001) surface. It is clear that between −7.9 and 0.2 eV, Ti 3d, O 2p, and C 2p states were strongly hybridized. The C 2p states around the Fermi level incorporated new energy states, which could be quite useful for the charge separation and charge transport. The Ti 3d states are missing in the lower CB. The hybridization between the C 2p and Ti 3d was observed in the upper CB, while the lower CB was populated by the empty C 2p states. In this regard, these empty C 2p states can directly accept the photoinduced electrons from the Ti 3d or O 2p upon excitation. Based on the DFT results, it can be predicted that CQDs will incorporate new energy states around the Fermi level in TiO_2, which will not only

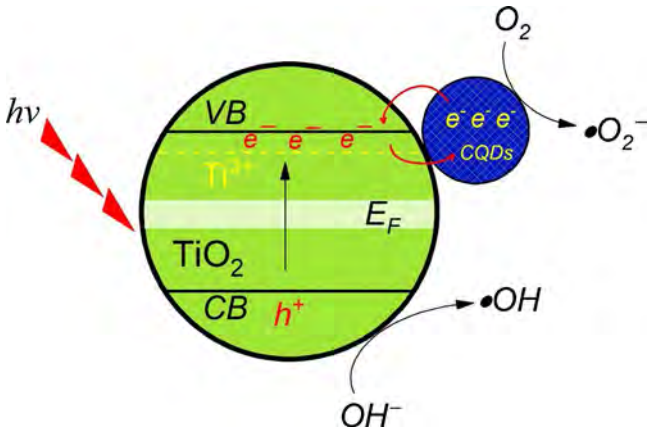

Fig. 11. Schematic illustration of the surface interaction between CQDs and TiO_2 NPs, which incorporate charge excitation in TiO_2 under light illumination and transfer between CQDs and TiO_2.

shrink the optical bandgap, but also can provide trap sites (acceptor states) for photogenerated electrons, enhancing the charge separation process. Both of these properties will improve the photocatalytic performance of CQDs decorated TiO_2 nanocomposite.

3.7. Proposed mechanism

The experimental results and theoretical calculations enable us to anticipate a proposed mechanism for the better charge separation and improved photocatalytic activity of CQDs/TiO_2 nanocomposites. A schematic view of charge excitation and transfer in CQDs and TiO_2 nanocomposite is given in Fig. 11. Due to undercoordinated Ti_{5c} atoms of TiO_2 (001) surface, more dioxygen derived oxygen atoms will be adsorbed on TiO_2 NPs with exposed {001} facets. Therefore, it is anticipated that the interfacial charge transfer will be improved, which will ultimately benefit the separation of hole-electron pair's. The adsorption of CQDs on TiO_2 produces a strong hybridization involving the CB of TiO_2 and π electrons of the aromatic rings present in the CQDs framework, which increases the light absorption. Also, the C 2p states of CQDs incorporate new energy states within the lower CB, which shrinks the bandgap. Therefore, the bandgap of CQDs/TiO_2 will end up narrower than pure TiO_2. The new states within the CB will behave as a reservoir for the photoinduced electrons in the nanocomposites, which might improve the charge separation process. This behavior was observed in the UV–vis and PL studies, while the origin was verified from the DFT calculations of the interface. These results suggested that CQDs can improve the charge separation and light-harvesting properties of TiO_2. The photodegradation experiment indicated a significant difference in the photodegradation efficiency of CQDs/TiO_2 for benzene, p-xylene, and toluene. The calculated adsorption energy of toluene is higher than benzene and p-xylene on TiO_2 (001) surface. Also, toluene demonstrated the ease in photodegrading compared to p-xylene and benzene. Although the calculations were carried out only for the TiO_2 (001) surface, it is predictable that these molecules will behave similarly regarding (101) surface. At first, the gaseous pollutants are adsorbed on CQDs/TiO_2 NPs. The adsorption experiment confirmed that CQDs improved the adsorption of benzene ring containing VOCs. Under UV–vis light illumination, the photoinduced electrons are excited to the CB as the holes migrate within the VB. The photoexcited electrons and holes generate $^{\cdot}OH$ and $O_2^{\cdot-}$ radicals that have been confirmed from the ESR results. The results recommended that more $O^{\cdot}H$ radicals are generated in CQDs/TiO_2 when compared with bare TiO_2. These $^{\cdot}OH$ and $O_2^{\cdot-}$ radicals further facilitated the efficient degradation of mixed gas phase VOCs.

4. Conclusion

A facile approach was used to prepare CQDs decorated TiO_2 nanocomposites. The variation in calcination temperature affected the overall photocatalytic activity of CQDs decorated TiO_2 nanocomposites, which led us to an optimum calcination temperature for better photocatalytic performance. CQDs decorated TiO_2 nanocomposites revealed two essential aspects in the photodegradation of gas-phase mixed VOCs. First, the hole-electron separation and light absorption properties were significantly improved compared to pure TiO_2, which were confirmed by the PL and visible light photodegradation activity tests. Second, the adsorption capability for the pollutant gas molecules was enhanced. The first principle calculations further confirmed the critical role of CQDs and the TiO_2 interface. For example, the new energy states induced by the C 2p of CQDs framework evidenced the origin of enhanced hole-electron separation compared to pure TiO_2. The computational analysis also differentiated the interaction among different aromatic rings containing VOCs with TiO_2 (001) surface, which might affect their photodegradation reaction. This study report in detail for the first time the potency of CQDs/TiO_2 nanocomposites for the mixed gas-phase volatile organic compounds photodegradation, which is important for the future designing of clean, inexpensive, and efficient photocatalysts.

CRediT authorship contribution statement

Asad Mahmood: Conceptualization, Methodology, Data curation, Writing - original draft. **Gansheng Shi:** Formal analysis. **Zepeng Rao:** Formal analysis. **Wang Xiao:** Data curation, Formal analysis. **Xiaofeng Xie:** Supervision. **Jing Sun:** Supervision.

Declaration of Competing Interest

The authors declare that they have no known competing financial interests or personal relationships that could have appeared to influence the work reported in this paper.

Acknowledgments

The authors are thankful for the financial support under the CAS President's International Fellowship Initiative (PIFI)program (2018PE0014), Shanghai “Belt and Road” Program for Young Foreign Scientists (17520742600), National Key Research and Development Program of China (2016YFA0203000), NSFC-DFG bilateral organization program (51761135107), Shanghai Sailing Program (18YF1426800), Scientific Research Program of Science and Technology Commission of Shanghai Municipality (19DZ1202600) and the Innovation Program of Shanghai Institute of Ceramics, Chinese Academy of Sciences.

Appendix A. Supplementary data

Supplementary material related to this article can be found, in the online version, at doi:https://doi.org/10.1016/j.jhazmat.2020.123402.

References

Abdol, M.A., Sadeghzadeh, S., Jalaly, M., Khatibi, M.M., 2019. Constructing a three-dimensional graphene structure via bonding layers by ion beam irradiation. Sci. Rep. 9 (1), 8127.
Bai, Y., Zhou, Y., Zhang, J., Chen, X., Zhang, Y., Liu, J., Wang, J., Wang, F., Chen, C., Li, C., Li, R., Li, C., 2019. Homophase junction for promoting spatial charge separation in photocatalytic water splitting. ACS Catal. 9 (4), 3242–3252.
Baker, S.N., Baker, G.A., 2010. Luminescent carbon nanodots: emergent nanolights. Angew. Chem. Int. Ed. Engl. 49 (38), 6726–6744.
Bharti, B., Kumar, S., Lee, H.N., Kumar, R., 2016. Formation of oxygen vacancies and Ti (3+) state in TiO_2 thin film and enhanced optical properties by air plasma treatment. Sci. Rep. 6, 32355.
Bianchi, C.L., Gatto, S., Pirola, C., Naldoni, A., Di Michele, A., Cerrato, G., Crocellà, V., Capucci, V., 2014. Photocatalytic degradation of acetone, acetaldehyde and toluene

in gas-phase: comparison between nano and micro-sized TiO_2. Appl. Catal. B: Environ. 146, 123–130.
Broday, D., Dayan, U., Aharonov, E., Laufer, D., Adel, M., 2020. Emissions from gas processing platforms to the atmosphere-case studies versus benchmarks. Environ. Impact Assess. Rev. 80, 106313.
Challagulla, S., Tarafder, K., Ganesan, R., Roy, S., 2017. Structure sensitive photocatalytic reduction of nitroarenes over TiO_2'. Sci. Rep. 7 (1), 8783.
Chen, M., Ma, J., Zhang, B., Wang, F., Li, Y., Zhang, C., He, H., 2018. Facet-dependent performance of anatase TiO_2 for photocatalytic oxidation of gaseous ammonia. Appl. Catal. B: Environ. 223, 209–215.
Debono, O., Hequet, V., Le Coq, L., Locoge, N., Thevenet, F., 2017. VOC ternary mixture effect on ppb level photocatalytic oxidation: removal kinetic, reaction intermediates and mineralization. Appl. Catal. B: Environ. 218, 359–369.
Di, J., Xia, J., Ji, M., Wang, B., Yin, S., Zhang, Q., Chen, Z., Li, H., 2015. Carbon quantum dots modified biocl ultrathin nanosheets with enhanced molecular oxygen activation ability for broad spectrum photocatalytic properties and mechanism insight. ACS Appl. Mater. Interfaces 7 (36), 20111–20123.
Di, J., Xia, J., Ji, M., Wang, B., Yin, S., Xu, H., Chen, Z., Li, H., 2016. Carbon quantum dots induced ultrasmall bioi nanosheets with assembled hollow structures for broad spectrum photocatalytic activity and mechanism insight. Langmuir 32 (8), 2075–2084.
Etacheri, V., Seery, M.K., Hinder, S.J., Pillai, S.C., 2010. Highly visible light active $TiO_{2-x}N_x$ heterojunction photocatalysts. Chem. Mater. 22 (13), 3843–3853.
Ferrighi, L., Datteo, M., Fazio, G., Di Valentin, C., 2016. Catalysis under cover: enhanced reactivity at the interface between (doped) graphene and anatase TiO_2. J. Am. Chem. Soc. 138 (23), 7365–7376.
Fu, S., Zheng, Y., Zhou, X., Ni, Z., Xia, S., 2019. Visible light promoted degradation of gaseous volatile organic compounds catalyzed by Au supported layered double hydroxides: influencing factors, kinetics and mechanism. J. Hazard. Mater. 363, 41–54.
Gao, H., Li, X., Lv, J., Liu, G., 2013. Interfacial charge transfer and enhanced photocatalytic mechanisms for the hybrid graphene/anatase TiO_2(001) nanocomposites. J. Phys. Chem. C 117 (31), 16022–16027.
Hu, Y., Xie, X., Wang, X., Wang, Y., Zeng, Y., Pui, D.Y.H., Sun, J., 2018. Visible-light upconversion carbon quantum dots decorated TiO_2 for the photodegradation of flowing gaseous acetaldehyde. Appl. Surf. Sci. 440, 266–274.
Huang, Y., Liang, Y., Rao, Y., Zhu, D., Cao, J.J., Shen, Z., Ho, W., Lee, S.C., 2017. Environment-friendly carbon quantum dots/$ZnFe_2O_4$ photocatalysts: characterization, biocompatibility, and mechanisms for no removal. Environ. Sci. Technol. 51 (5), 2924–2933.
Ji, J., Xu, Y., Huang, H., He, M., Liu, S., Liu, G., Xie, R., Feng, Q., Shu, Y., Zhan, Y., Fang, R., Ye, X., Leung, D.Y.C., 2017. Mesoporous TiO_2 under Vuv irradiation: enhanced photocatalytic oxidation for VOCs degradation at room temperature. Chem. Eng. J. 327, 490–499.
Jing, S., Zhao, Y., Sun, R.-C., Zhong, L., Peng, X., 2019. Facile and high-yield synthesis of carbon quantum dots from biomass-derived carbons at mild condition. ACS Sustain. Chem. Eng. 7 (8), 7833–7843.
Jones, L.A., Ott, A., Tardio, J., Morrison, P., Rosenberg, S., Gunda, M., Bhargava, S.K., 2014. VOC emission from alumina calcination stacks caused by thermal decomposition of organic additives. J. Environ. Chem. Eng. 2 (1), 626–631.
Lee, S.M., Hwang, I.-H., Lee, D.Y., Kim, S.S., 2020. A new combined electrolysis and catalytic system for removal of VOCS. Chem. Eng. J. 382, 123032.
Li, H., Shi, W., Huang, W., Yao, E.P., Han, J., Chen, Z., Liu, S., Shen, Y., Wang, M., Yang, Y., 2017a. Carbon quantum dots/TiO_x electron transport layer boosts efficiency of planar heterojunction perovskite solar cells to 19. Nano Lett. 17 (4), 2328–2335.
Li, M., Lu, B., Ke, Q.F., Guo, Y.J., Guo, Y.P., 2017b. Synergetic effect between adsorption and photodegradation on nanostructured TiO_2/Activated carbon fiber felt porous composites for toluene removal. J. Hazard. Mater. 333, 88–98.
Li, Y., Liu, Z., Wu, Y., Chen, J., Zhao, J., Jin, F., Na, P., 2018. Carbon dots-TiO_2 nanosheets composites for photoreduction of Cr(Vi) under sunlight illumination: favorable role of carbon dots. Appl. Catal. B: Environ. 224, 508–517.
Liang, W.J., Li, J., Jin, Y.Q., 2010. Photocatalytic degradation of gaseous acetone, toluene, and p-xylene using a TiO_2 Thin Film'. J. Environ. Sci. Health A. Tox. Subst. Environ. Eng. 45 (11), 1384–1390.
Liang, Z., Hou, H., Fang, Z., Gao, F., Wang, L., Chen, D., Yang, W., 2019. Hydrogenated TiO_2 nanorod arrays decorated with carbon quantum dots toward efficient photoelectrochemical water splitting. ACS Appl. Mater. Interfaces 11 (21), 19167–19175.
Lim, S.Y., Shen, W., Gao, Z., 2015. Carbon quantum dots and their applications. Chem. Soc. Rev. 44 (1), 362–381.
Lin, W., Xie, X., Wang, X., Wang, Y., Segets, D., Sun, J., 2018. Efficient adsorption and sustainable degradation of gaseous acetaldehyde and o-xylene using rGO-TiO_2 photocatalyst. Chem. Eng. J. 349, 708–718.
Luo, Y., Ollis, D.F., 1996. Heterogeneous photocatalytic oxidation of trichloroethylene and toluene mixtures in air: kinetic promotion and inhibition, time-dependent catalyst activity. J. Catal. 163, 1–11.
Ma, Y., Li, X., Yang, Z., Xu, S., Zhang, W., Su, Y., Hu, N., Lu, W., Feng, J., Zhang, Y., 2016. Morphology control and photocatalysis enhancement by in situ hybridization of cuprous oxide with nitrogen-doped carbon quantum dots. Langmuir 32 (37), 9418–9427.
Martindale, B.C., Hutton, G.A., Caputo, C.A., Reisner, E., 2015. Solar hydrogen production using carbon quantum dots and a molecular nickel catalyst. J. Am. Chem. Soc. 137 (18), 6018–6025.
Moulis, F., Krýsa, J., 2013. Photocatalytic degradation of several VOCs (n-hexane, n-butyl acetate and toluene) on TiO_2 layer in a closed-loop reactor. Catal. Today 209, 153–158.
Munoz, R., Souza, T.S., Glittmann, L., Perez, R., Quija, G., 2013. Biological anoxic treatment of O(2)-free VOC emissions from the petrochemical industry: a proof of concept study. J. Hazard. Mater. 260, 442–450.
Mustafa, M.F., Fu, X., Liu, Y., Abbas, Y., Wang, H., Lu, W., 2018. Volatile organic compounds (VOCs) removal in non-thermal plasma double dielectric barrier discharge reactor. J. Hazard. Mater. 347, 317–324.
Naldoni, A., Altomare, M., Zoppellaro, G., Liu, N., Kment, S., Zboril, R., Schmuki, P., 2019. Photocatalysis with reduced TiO_2: from black TiO_2 to cocatalyst-free hydrogen production'. ACS Catal. 9 (1), 345–364.
Nie, L., Duan, B., Lu, A., Zhang, L., 2018. Pd/TiO_2@carbon microspheres derived from chitin for highly efficient photocatalytic degradation of volatile organic compounds. ACS Sustain. Chem. Eng. 7 (1), 1658–1666.
Peng, H., Travas-Sejdic, J., 2009. Simple aqueous solution route to luminescent carbogenic dots from carbohydrates. Chem. Mater. 21 (23), 5563–5565.
Petronella, F., Truppi, A., Ingrosso, C., Placido, T., Striccoli, M., Curri, M.L., Agostiano, A., Comparelli, R., 2017. Nanocomposite materials for photocatalytic degradation of pollutants. Catal. Today 281, 85–100.
Pradhan, A.C., Uyar, T., 2019. Electrospun Fe_2O_3 entrenched SiO_2 supported N and S dual incorporated TiO_2 nanofibers derived from mixed polymeric template/surfactant: enriched mesoporosity within nanofibers, effective charge separation, and visible light photocatalysis activity. Ind. Eng. Chem. Res. 58 (28), 12535–12550.
Ramimoghadam, D., Bagheri, S., Abd Hamid, S.B., 2014. Biotemplated synthesis of anatase titanium dioxide nanoparticles via lignocellulosic waste material. Biomed Res. Int. 2014, 205636.
Rao, Z., Xie, X., Wang, X., Mahmood, A., Tong, S., Ge, M., Sun, J., 2019. Defect chemistry of Er^{3+}-Doped TiO_2 and its photocatalytic activity for the degradation of flowing gas-phase VOCs. J. Phys. Chem. C 123 (19), 12321–12334.
Sauer, Michael L., Hale, Michael A., Ollis, D.F., 1995. Heterogeneous photocatalytic oxidation of dilute toluene-chlorocarbon mixtures in air. J. Photochem. Photobiol. A: Chem. 88, 169–178.
Shen, X., Dong, G., Wang, L., Ye, L., Sun, J., 2019. Enhancing photocatalytic activity of no removal through an in situ control of oxygen vacancies in growth of TiO_2. Adv. Mater. Interfaces 6 (19), 1901032.
Shi, Y., Chen, J., Mao, Z., Fahlman, B.D., Wang, D., 2017. Construction of z-scheme heterostructure with enhanced photocatalytic H_2 evolution for G-C_3N_4 nanosheets via loading porous silicon. J. Catal. 356, 22–31.
Suárez, S., Jansson, I., Ohtani, B., Sánchez, B., 2019. From titania nanoparticles to decahedral anatase particles: photocatalytic activity of TiO_2/zeolite hybrids for VOCs oxidation. Catal. Today 326, 2–7.
Tofighi, G., Yu, X., Lichtenberg, H., Doronkin, D.E., Wang, W., Wöll, C., Wang, Y., Grunwaldt, J.-D., 2019. Chemical nature of microfluidically synthesized aupd nanoalloys supported on TiO_2. ACS Catal. 9 (6), 5462–5473.
Wang, C., Xi, J.Y., Hu, H.Y., Yao, Y., 2009. Advantages of combined UV photodegradation and biofiltration processes to treat gaseous chlorobenzene. J. Hazard. Mater. 171 (1–3), 1120–1125.
Wang, J., Han, F., Rao, Y., Hu, T., Huang, Y., Cao, J.-j., Lee, S.C., 2018. Visible-light-driven nitrogen-doped carbon quantum dots/$CaTiO_3$ composite catalyst with enhanced no adsorption for no removal. Ind. Eng. Chem. Res. 57 (31), 10226–10233.
Wang, F., Wu, Y., Wang, Y., Li, J., Jin, X., Zhang, Q., Li, R., Yan, S., Liu, H., Feng, Y., Liu, G., Lv, W., 2019. Construction of novel z-scheme nitrogen-doped carbon dots/{001} TiO_2 nanosheet photocatalysts for broad-spectrum-driven diclofenac degradation: mechanism insight, products and effects of natural water matrices. Chem. Eng. J. 356, 857–868.
Wang, M., Tan, S., Kan, S., Wu, Y., Sang, S., Liu, K., Liu, H., 2020. In-situ assembly of TiO_2 with high exposure of (001) facets on three-dimensional porous graphene aerogel for lithium-sulfur battery. J. Energy Chem. 49, 316–322.
Weon, S., Choi, J., Park, T., Choi, W., 2017. Freestanding doubly open-ended TiO_2 nanotubes for efficient photocatalytic degradation of volatile organic compounds. Appl. Catal. B: Environ. 205, 386–392.
Weon, S., Kim, J., Choi, W., 2018. Dual-components modified TiO_2 with Pt and fluoride as deactivation-resistant photocatalyst for the degradation of volatile organic compound. Appl. Catal. B: Environ. 220, 1–8.
Yang, Y., Ye, K., Cao, D., Gao, P., Qiu, M., Liu, L., Yang, P., 2018. Efficient charge separation from F(-) selective etching and doping of anatase-TiO_2{001} for enhanced photocatalytic hydrogen production. ACS Appl. Mater. Interfaces 10 (23), 19633–19638.
Yao, P., Liu, H., Wang, D., Chen, J., Li, G., An, T., 2018. Enhanced visible-light photocatalytic activity to volatile organic compounds degradation and deactivation resistance mechanism of titania confined inside a metal-organic framework. J. Colloid Interface Sci. 522, 174–182.
Zhang, X., Gao, B., Creamer, A.E., Cao, C., Li, Y., 2017. Adsorption of VOCs onto engineered carbon materials: a review. J. Hazard. Mater. 338, 102–123.
Zheng, S., Xu, X., Zhang, Y., Wang, L., Yang, Y., Jin, S., Yang, X., 2019. Characteristics and sources of VOCs in urban and suburban environments in Shanghai, China, during the 2016 G20 Summit. Atmos. Pollut. Res. 10 (6), 1766–1779.
Zhou, Y., Yang, S., Fan, D., Reilly, J., Zhang, H., Yao, W., Huang, J., 2019. Carbon quantum dot/TiO2 nanohybrids: efficient photocatalysts for hydrogen generation via intimate contact and efficient charge separation. ACS Appl. Nano Mater. 2 (2), 1027–1032.
Zhu, L., Shen, D., Luo, K.H., 2020. A critical review on vocs adsorption by different porous materials: species, mechanisms and modification methods. J. Hazard. Mater. 389, 122102.
Zorn, M.E., Hay, S.O., Anderson, M.A., 2010. Effect of molecular functionality on the photocatalytic oxidation of gas-phase mixtures. Appl. Catal. B: Environ. 99 (3–4), 420–427.
Zou, W., Gao, B., Ok, Y.S., Dong, L., 2019. Integrated adsorption and photocatalytic degradation of volatile organic compounds (VOCs) using carbon-based nanocomposites: a critical review. Chemosphere 218, 845–859.